Supplement of Atmos. Chem. Phys., 25, 881–903, 2025
https://doi.org/10.5194/acp-25-881-2025-supplement

Atmospheric Chemistry and Physics Open Access

Supplement of

The surface tension and cloud condensation nuclei (CCN) activation of sea spray aerosol particles

Judith Kleinheins et al.

Correspondence to: Judith Kleinheins (judith.kleinheins@env.ethz.ch)

Contents

S1 Influence of the Sigmoid parameter d

To test the influence of the parameter d on the critical supersaturation we calculated Köhler curves with Eq. 1. We assumed the particle to consist entirely of an organic (surface-active) substance, i.e., it contains no inorganic co-solute. We further assumed solution ideality, i.e., $a_w = x_w$, where x_w is the mole fraction of water and the organic substance is assumed not to dissociate. The surface tension σ in the Kelvin equation (exponential function in Eq. 1) is calculated as a function of the total composition of the particle using the Sigmoid model (Eq. 2). As such, no bulk depletion is considered. The temperature is set to $T = 25\,°\mathrm{C}$ and the molar volume of water to $v_i N_A = 18.05\,\mathrm{cm^3\,mol^{-1}}$. In Fig. S1, the results are shown for three different substances, i.e., propionic acid, SDS, and oleic acid, which are covering a broad range of p values. The values for p, σ_i, and $v_i N_A$ which were used for each substance are annotated in the respective panel. The curves with $d = 1$ are highlighted by a thicker, black line because the Eberhart model is a simplified version of the Sigmoid model with $d = 1$.

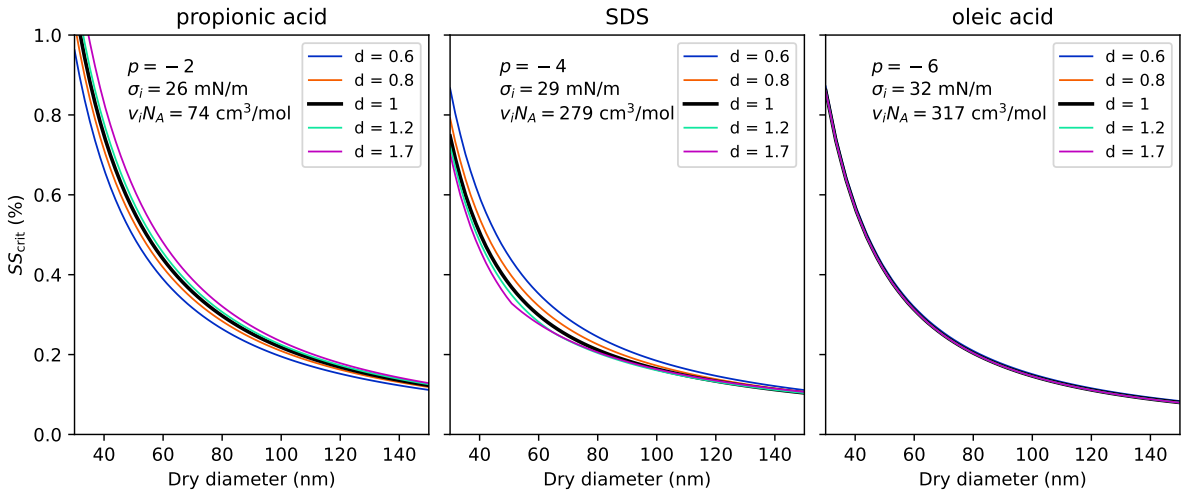

Figure S1: Influence of the Sigmoid model's parameter d: Critical supersaturation as a function of the dry diameter for three different substances and 5 different values for d.

It can be seen that the curves for the various d values are close to each other and in the case of oleic acid overlap entirely. The strongest influence of d on SS_{crit} is observed for the case with SDS. According to the fits with the Sigmoid model in El Haber et al. (2024), $d = 1.65$ for SDS and small dry diameters. For dry diameters between 30 nm and 60 nm, assuming $d = 1$ leads to an error in $\Delta SS_{\mathrm{crit}}$ of $\approx 0.05\,\%$. This error can be regarded as the maximum overall error, since here we assumed particles consisting entirely of the surfactant and bulk depletion is not considered, both of which enhance the surface tension lowering effect on SS_{crit}. This small maximum error justifies the assumption of $d = 1$ in the Eberhart model for the purpose of calculating SS_{crit}.

S2 Computational flowchart for the quaternary Eberhart –Monolayer model

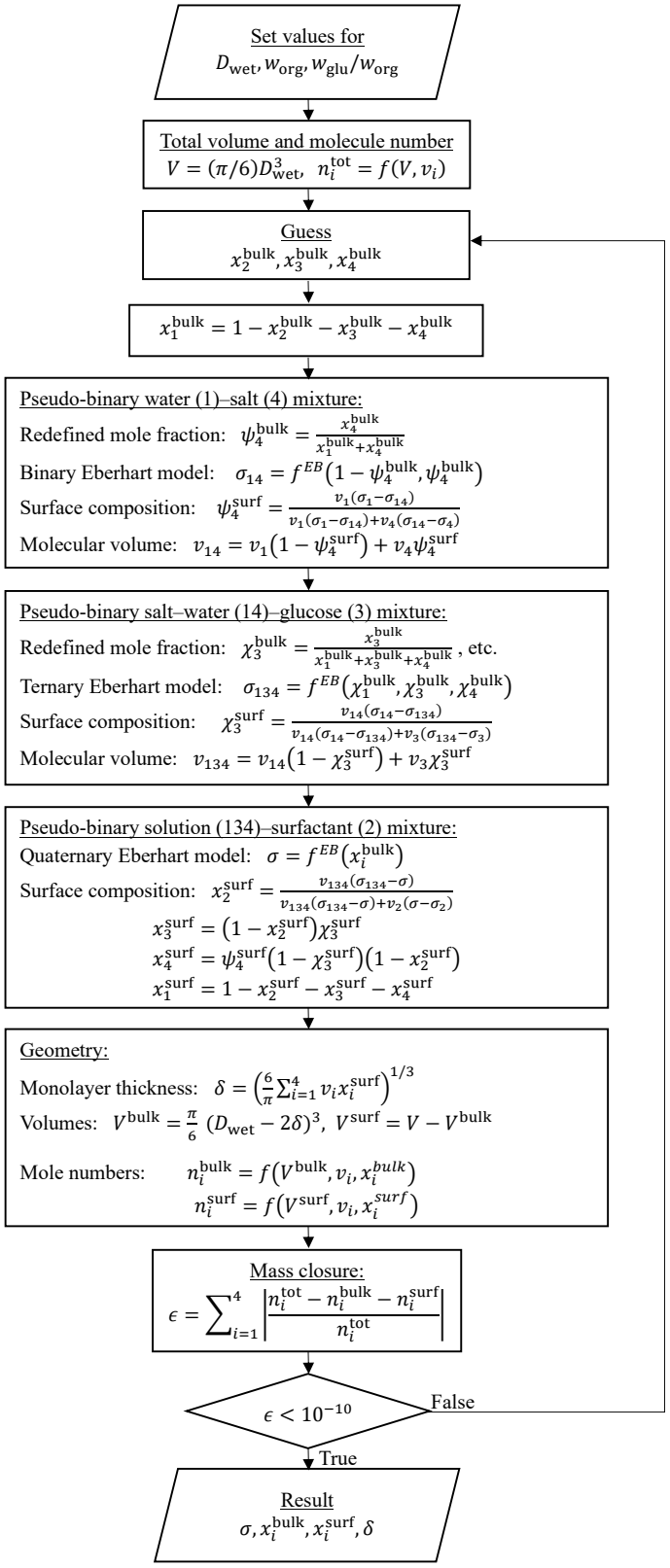

Figure S2: Flowchart for calculating bulk–surface partitioning with the Eberhart–Monolayer model for a quaternary mixture.

S3 Comparison to surface tension data of small droplets

Bain et al. (2023) performed surface tension measurements of $6-9\,\mu$m radius droplets containing one or two surfactants and a co-solute, i.e., NaCl or glutaric acid. In the same study, they combined the Monolayer model to describe partitioning with a Szyszkowski-Langmuir type equation for the surface tension isotherm to predict the surface tension of the small droplets. Similarly, here we compare our model, which uses the multi-component Eberhart model instead of the Szyszkowski–Langmuir type model, with their measurements. The results are shown in Fig. S3. Densities and molar masses were taken from Table S6 in the Supporting Information of Bain et al. (2023). The pure component surface tension of the surfactant σ_2 was chosen to be equal to the surface tension of the binary water–surfactant solution at concentrations higher than the CMC. The binary separation factor of the surfactant in water S_{12} was determined by fitting the binary Eberhart model to binary water–surfactant surface tension data measured by Bain et al. (2023). Salting-out factors A_{23}^{SO} and B_{23}^{SO} were chosen such that the ternary Eberhart model (black lines) matches the experimental bulk data by Bain et al. (2023) (black circles). These model parameters are given at the right side of each panel. Blue solid and dashed lines show the surface tension of $6\,\mu$m and $9\,\mu$m radius droplets predicted by the Eberhart–Monolayer model, respectively. Like the results by Bain et al. (2023), our model seems to predict a slightly too strong surface partitioning leading to lower surface tensions for small droplets in most cases, but the general trends are reproduced well.

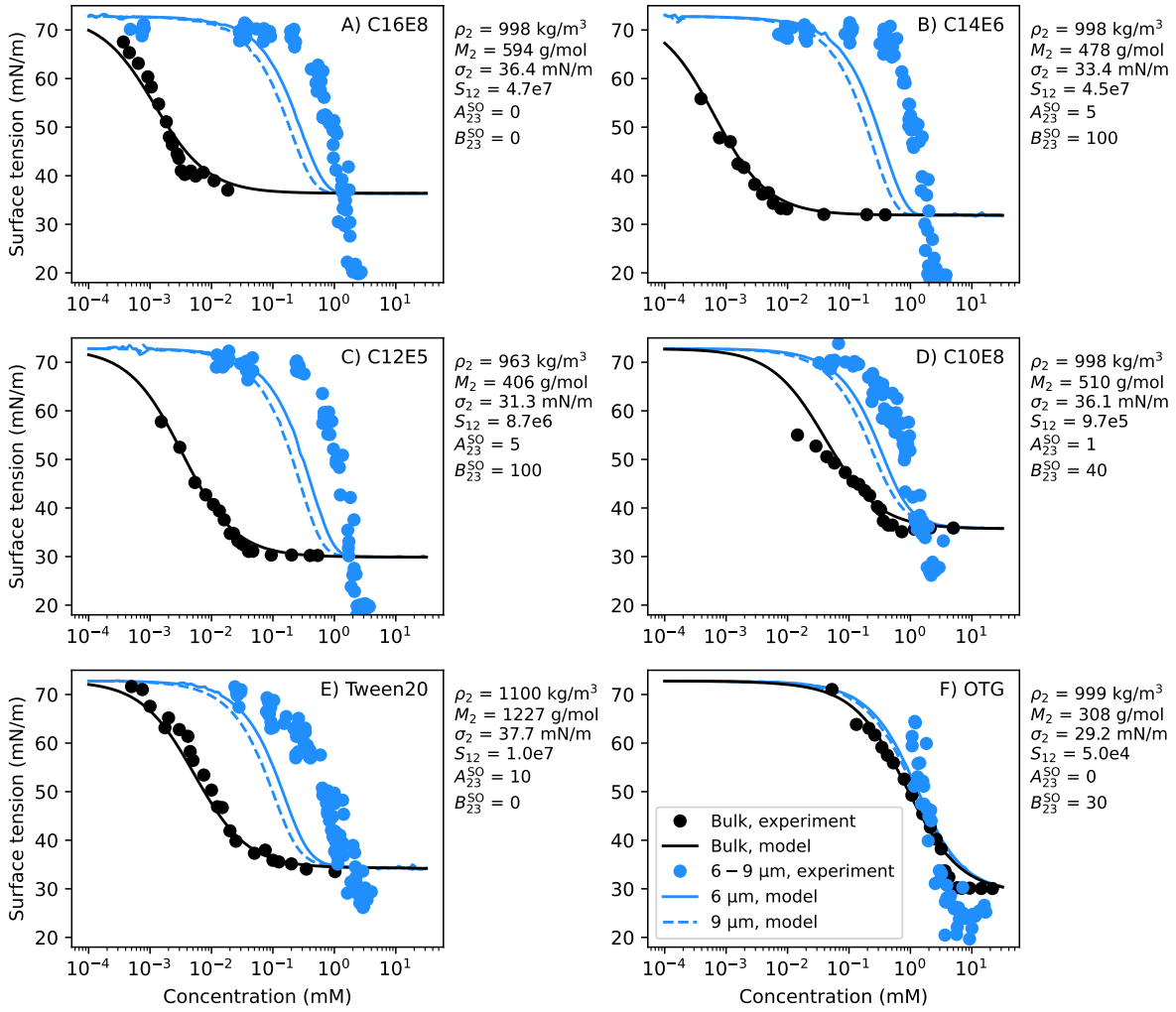

Figure S3: Comparison of the Eberhart–Monolayer model (lines) to surface tension measurements of droplets with a radius of $6-9\,\mu$m (blue circles) and large droplets ("Bulk", black circles) from Bain et al. (2023). The droplets contain 0.5 M NaCl and the surfactant annotated in the upper right corner of each panel. At the right side of each panel, the parameters used in the model for the respective surfactant are given.

S4 Influence of solution non-ideality

The water activity (Raoult effect) plays an important role in the calculation of the critical supersaturation via Eq. 1. To test the sensitivity of SS_{crit} on the choice of a_w, Köhler curves were constructed based on four different ways to calculate a_w.

First, an ideal solution is assumed, i.e., $a_w = \hat{x}_w$, where $\hat{x}_w$ is calculated based on the dissociation of NaCl into 2 ions and no dissociation of the organic substances (labelled "ideal").

Second, to consider solution non-ideality, a_w is calculated with AIOMFAC. Note that liquid–liquid phase separation is not considered in that calculation, i.e., all substances are forced to be in one phase. We label this second approach "AIOMFAC-1ph".

Third, we calculate a_w assuming that the surfactant is hydrophobic and therefore entirely present in a separate phase, e.g., in the form of micelles or as a surface layer (labelled "surfactant hydrophobic"). In this case, the surfactant is not contributing to the Raoult effect, i.e., the bulk mole fractions are converted to "surfactant-free" mole fractions $\tilde{x}$. For a system of water(1)–surfactant(2)–glucose(3)–NaCl(4), for example, the surfactant-free mole fraction of water would be calculated as $\tilde{x}_1 = x_1/(x_1 + x_3 + x_4)$. Based on $\tilde{x}_1$,$\tilde{x}_3$, and $\tilde{x}_4$, a_w is calculated with AIOMFAC. We label this third approach as "surfactant hydrophobic".

Fourth, we combine the "surfactant hydrophobic" case with AIOMFAC-1ph by taking the minimum a_w of both.

To test their influence, we use all four assumptions to calculate Köhler curves with either

1. the Eberhart–Monolayer model (a_w is calculated based on x_i^{bulk}, $\sigma = f(x_i^{\mathrm{bulk}})$,
2. a calculation neglecting bulk depletion (a_w is calculated based on x_i^{tot}, $\sigma = f(x_i^{\mathrm{tot}})$, and
3. Classical Köhler theory (a_w is calculated based on x_i^{tot}, $\sigma = \sigma_1$).

The result of this comparison for an SDS–NaCl particle of $D_{\mathrm{dry}} = 50$ nm particle with medium organic content is shown in Fig. S4. In the second row of all three columns, it can be seen that a_w predicted with AIOMFAC-1ph (blue dashed line) is higher than the one assuming a hydrophobic surfactant (yellow dashed line) at low wet diameters. Therefore, the particle is assumed to undergo LLPS in that range and the best estimate (black solid line) follows the "surfactant hydrophobic" calculation. As soon as AIOMFAC-1ph predicts a lower a_w than "surfactant hydrophobic" (blue and yellow lines are crossing), the droplet is assumed to be one homogeneous phase, and the best estimate follows AIOMFAC-1ph. This results in a local maximum in a_w, which also shows up as a global maximum in the Köhler curve when using Classical Köhler theory (first row, right column) and marks SS_{crit} in that case (black circle). In the calculation using classical Köhler theory, the higher surface tension ($\sigma = \sigma_1$, see third row) leads to a higher Kelvin effect and a higher SS_{crit} than those resulting from the first two model approaches. Yet, in all three model approaches, SS_{crit} calculated considering non-ideality (black circles) is very similar to that assuming solution ideality (gray circles). This applies to most cases analyzed in this study.

Solution non-ideality only had a considerable influence on SS_{crit} when the dry diameter is small ($D_{\mathrm{dry}} = 50$ nm) and the organic fraction is high and has a low O:C ratio. Two such examples are shown in Fig. S5 and Fig. S6 for an SDS–glucose–NaCl particle ($w_{\mathrm{glu}}/w_{\mathrm{org}} = 0.05$) and a pinonic acid–NaCl particle, respectively, both having a high organic fraction and $D_{\mathrm{dry}} = 50$ nm. These two examples show that in cases with high organic fraction and small dry diameters, the particles undergo little hygroscopic growth and, as a result, are still in a phase-separated state at activation leading to increased SS_{crit} values compared to a calculation assuming ideality.

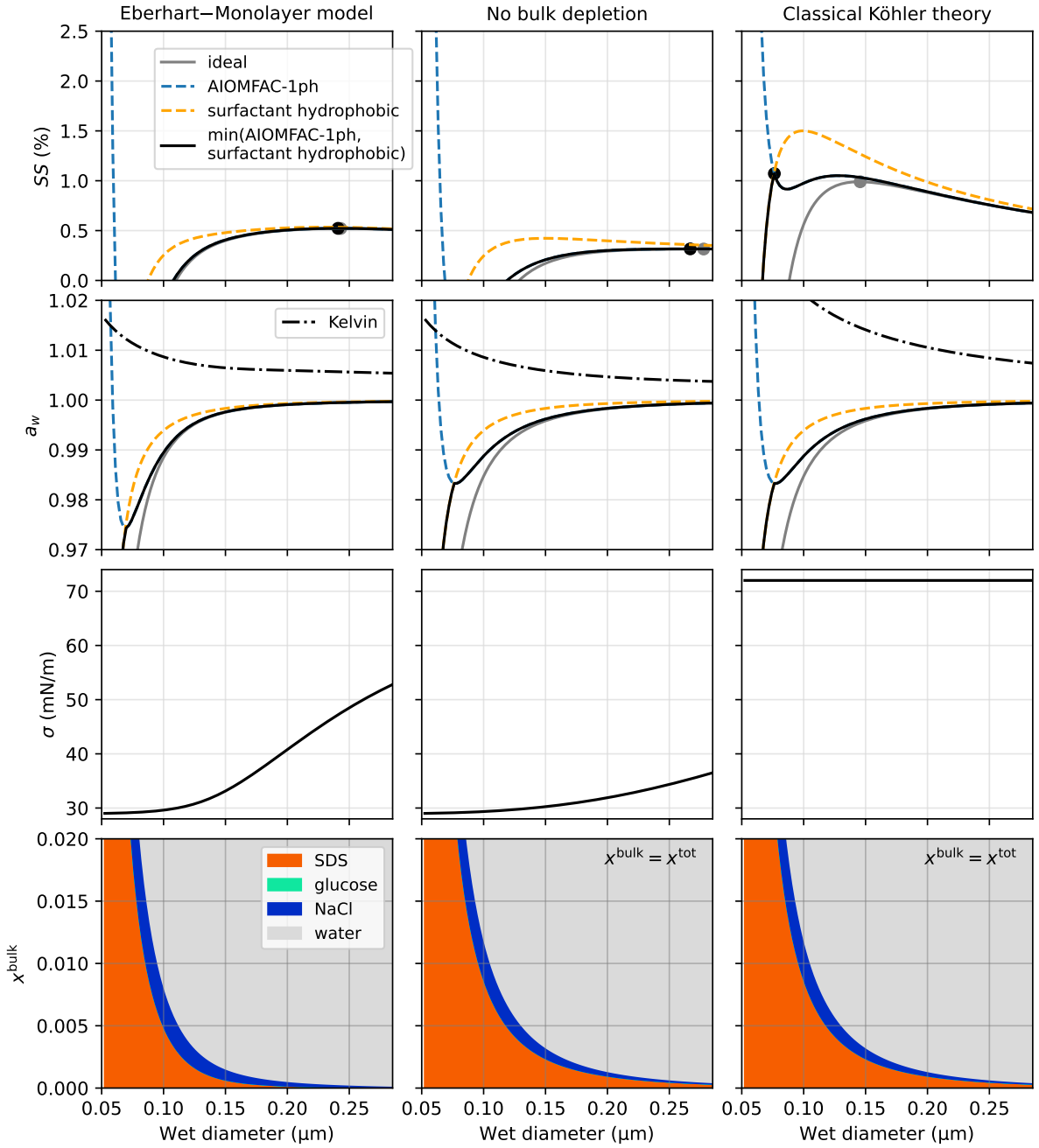

Figure S4: Four different ways of calculating the Raoult effect (see legend) in Köhler curves using three different model approaches (columns): with the Eberhart–Monolayer model, assuming no bulk depletion, and with Classical Köhler theory. Calculations are for an SDS–NaCl particle with $D_{\mathrm{dry}} = 50\,\mathrm{nm}$ with an organic fraction "med" ($w_{\mathrm{glu}}/w_{\mathrm{org}} = 0$). First row: Köhler curve and critical supersaturation (circle). Second row: water activity a_w (Raoult effect) and saturation ratio of the Kelvin effect, calculated with the exponential function in Eq. 1. Third row: droplet surface tension. Fourth row: bulk composition (first column) and total composition (second and third column). The y-axis range was limited to 0–0.02 for a better visibility of the solute share. SDS is represented with dodecanoic acid in AIOMFAC and assumed not to dissociate in Classical Köhler theory.

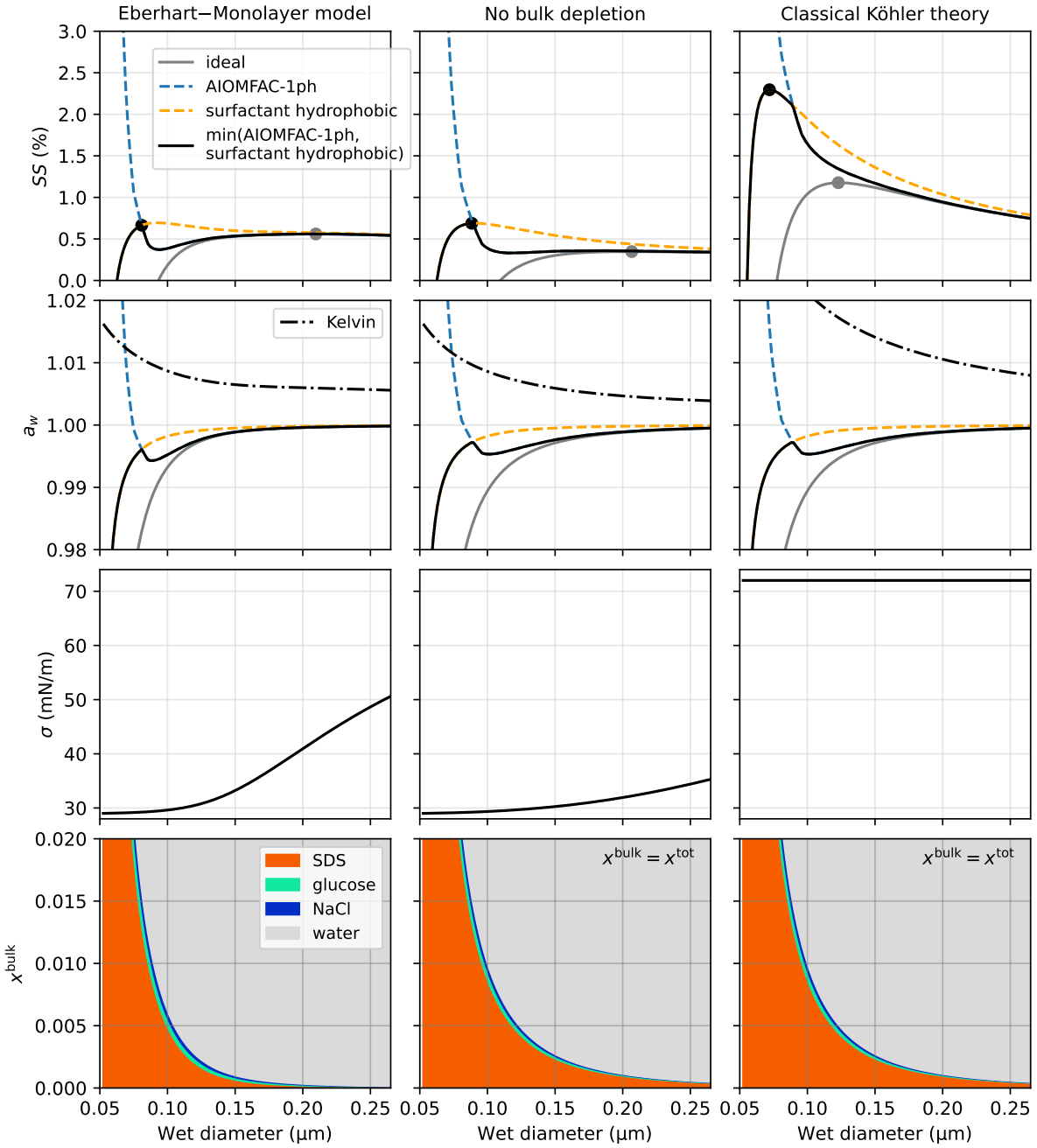

Figure S5: Four different ways of calculating the Raoult effect (see legend) in Köhler curves using three different model approaches (columns): with the Eberhart–Monolayer model, assuming no bulk depletion, and with Classical Köhler theory. Calculations are for an SDS–glucose–NaCl particle with $D_{dry} = 50\,nm$, organic fraction "high" and $w_{glu}/w_{org} = 0.05$. First row: Köhler curve and critical supersaturation (circle). Second row: water activity a_w (Raoult effect) and saturation ratio of the Kelvin effect, calculated with the exponential function in Eq. 1. Third row: droplet surface tension. Fourth row: bulk composition (first column) and total composition (second and third column). The y-axis range was limited to 0–0.02 for a better visibility of the solute share. SDS is represented with dodecanoic acid in AIOMFAC and assumed not to dissociate in Classical Köhler theory.

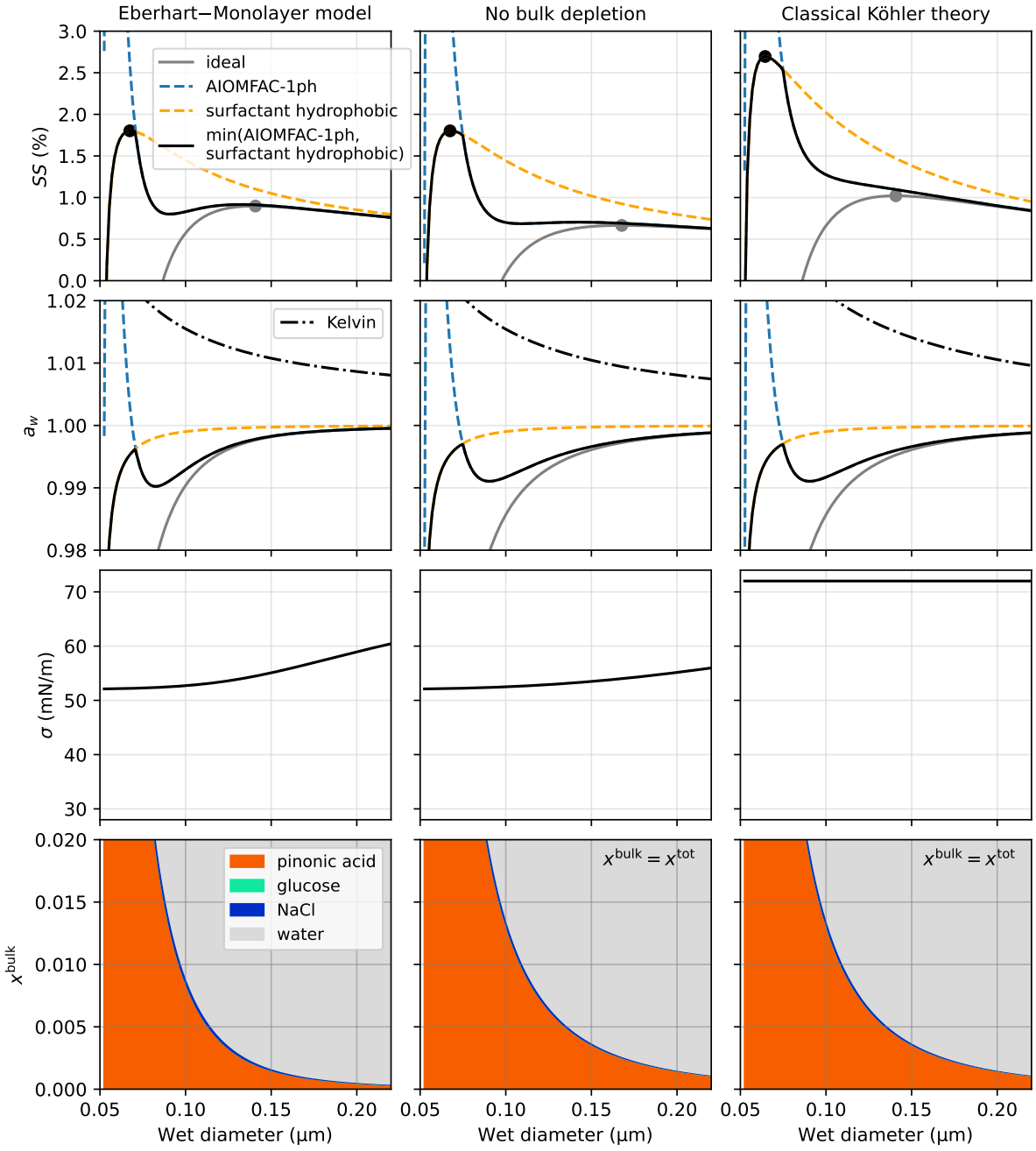

Figure S6: Four different ways of calculating the Raoult effect (see legend) in Köhler curves using three different model approaches (columns): with the Eberhart–Monolayer model, assuming no bulk depletion, and with Classical Köhler theory. Calculations are for a pinonic acid–NaCl particle with $D_{\mathrm{dry}} = 50\,\mathrm{nm}$ and an organic fraction "high" ($w_{\mathrm{glu}}/w_{\mathrm{org}} = 0$). First row: Köhler curve and critical supersaturation (circle). Second row: water activity a_w (Raoult effect) and saturation ratio of the Kelvin effect, calculated with the exponential function in Eq. 1. Third row: droplet surface tension. Fourth row: bulk composition (first column) and total composition (second and third column). The y-axis range was limited to 0–0.02 for a better visibility of the solute share.

S5 Influence of SDS dissociation

In past studies, sodium dodecyl sulfate (SDS) often was assumed to fully dissociate in solution (e.g., Sorjamaa et al., 2004; Prisle et al., 2010). In fact, SDS can undergo dissociation in aqueous solution, the degree of which depends on the degree of dilution in water, as well as on the relative ratio of NaCl and SDS (Matijević and Pethica, 1958). This raises the question of which van't Hoff factor should be used in calculations assuming solution ideality. Furthermore, SDS cannot be represented with the functional groups implemented in AIOMFAC, due to the organic-sulfate group, raising the question of how to implement solution non-ideality. To test the sensitivity of the critical supersaturation on the van't Hoff factor of SDS as well as its representation in AIOMFAC for solution non-ideality for the calculation of a_w, we tested three cases. First, we represented SDS by dodecanoic acid in AIOMFAC, which is a fatty acid with the same hydrocarbon chain length and an amphiphilic, non-dissociating molecule. Second, we assumed solution ideality with a van't Hoff factor of $\nu_{\mathrm{H,SDS}} = 1$. Third, we assumed full dissociation of SDS by using $\nu_{\mathrm{H,SDS}} = 2$. SS_{crit} for these cases and all three model approaches is shown in Fig. S7.

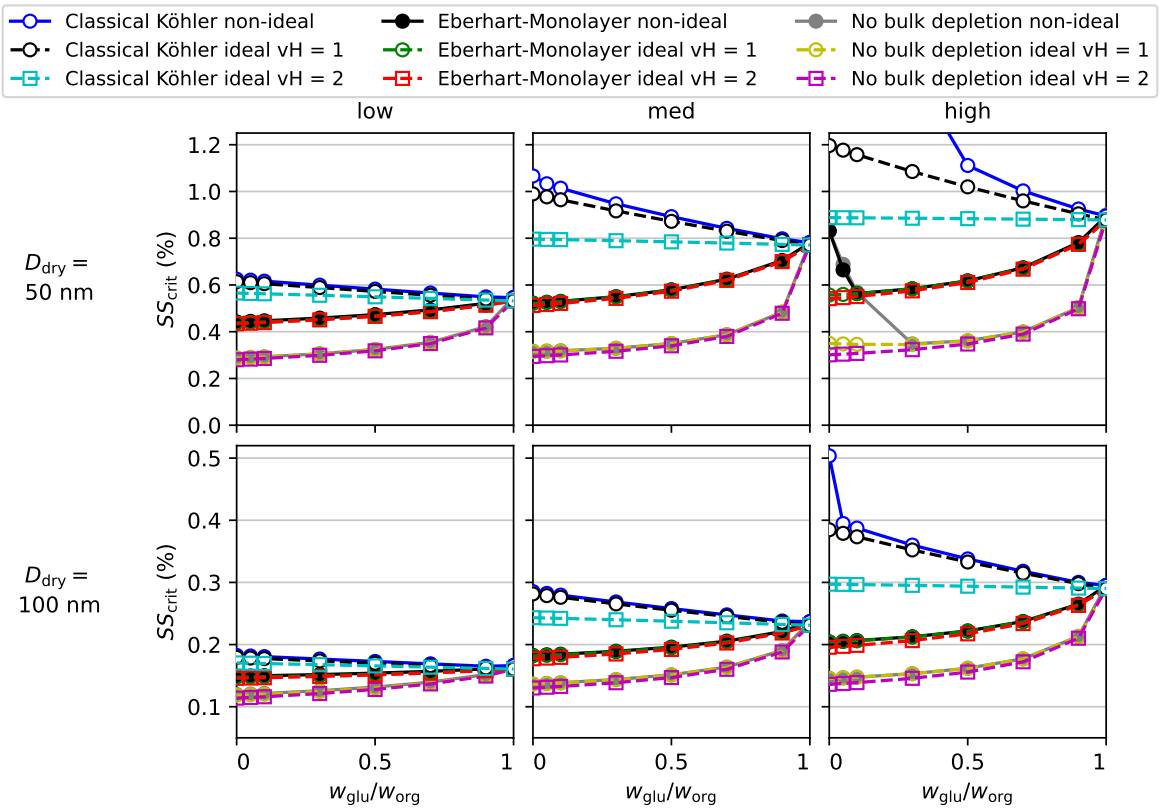

Figure S7: Influence of solution non-ideality and SDS dissociation on SS_{crit} of SDS–NaCl particles calculated with the three different model approaches (classical Köhler theory, the Eberhart–Monolayer model, and assuming no bulk depletion). In cases labelled "non-ideal", a_w is calculated using AIOMFAC (best estimate, see Sect. S4), with SDS being represented with dodecanoic acid (non-dissociating). Cases labelled "ideal" assume $\gamma_w = 1$, full dissociation of NaCl and either no dissociation of SDS ("vH = 1") or full dissociation of SDS ("vH = 2").

When using classical Köhler theory, a strong influence of solution non-ideality and the degree of dissociation of SDS on SS_{crit} is found, except for particles with $D_{\mathrm{dry}} = 100\,\mathrm{nm}$ and low organic content ($\Delta SS_{\mathrm{crit}} < 0.012\,\%$). In contrast, the influence of solution non-ideality and SDS dissociation on SS_{crit} is negligible in calculations with the Eberhart–Monolayer model or assuming no bulk depletion. Only at high SDS content (e.g., 98.8 % in dry mass), the critical supersaturation is much higher when representing SDS with dodecanoic acid due to LLPS. The reason of the higher influence of dissociation and non-ideality in classical Köhler theory is that all SDS is assumed to remain in the bulk thereby contributing to the Raoult effect. Furthermore, the lower surface tension in the other two model approaches leads to a stronger particle growth as a function of RH, such that at activation the Raoult effect is very close to 1 and less sensitive to the SDS representation in the model.

S6 Eberhart fit parameters of organic substances

The parameters σ_i and S_{1i} were determined for 76 organic substances based on the data compiled by El Haber et al. (2024) as follows. The pure component surface tension σ_i for each substance was calculated as an average of the experimental pure component surface tensions given in Tables 1-3 in El Haber et al. (2024). If no pure component surface tension is given by El Haber et al. (2024), σ_i was used as a fit parameter and determined together with S_{1i} by fitting the binary Eberhart model (Eq. 3) to experimental binary surface tension data provided by El Haber et al. (2024) in the supplement. For the fitting, all experimental datasets given in the supplement of El Haber et al. (2024) were considered that were also used by El Haber et al. (2024) when fitting the Sigmoid model to determine their recommended data. For example, for propionic acid, a binary Eberhart model fit was made to the combined experimental data from Alvarez et al. (1997), Granados et al. (2006), and Suárez and Romero (2011), as shown in Fig. S10 in the upper left panel.

Table S1: Eberhart fit parameters of acids shown in Fig. 3. Substances with a star correspond to those denoted by a star in Fig. 3. CI_{95} is the 95 % confidence interval of parameters that were fitted. References for σ_i values from measurements (i.e., that have no CI_{95} value) can be found in El Haber et al. (2024). RMSE is the root mean square error.

No.	name	S_{1i}	$CI_{95}(S_{1i})$	σ_i (mN m^{-1})	$CI_{95}(\sigma_i)$ (mN m^{-1})	σ_1 (mN m^{-1})	RMSE (mN m^{-1})
★	propionic acid	55.3	4.6	26.2		72.0	0.664
★	valeric acid	974.6	36.6	26.7		72.0	0.073
★	glutaric acid	67.3	10.5	53.1	0.8	72.0	0.026
★	pinonic acid	3.7e3	1.5e3	52.1	3.6	72.0	0.075
★	oleic acid	9.9e6	4.4e6	32.2		72.0	0.618
1	formic acid	5.4	0.5	37.5		72.0	0.014
2	acetic acid	15.6	1.3	27.9		72.0	0.257
3	butyric acid	199.2	12.1	26.2		72.0	0.053
4	oxalic acid	16.8	9.4	62.7	3.4	72.0	0.117
5	methanesulfonic acid	13.9	2.4	53.0		72.0	0.002
6	malonic acid	26.7	5.8	60.5	0.9	72.0	0.068
7	maleic acid	33.4	8.6	55.2	1.5	72.0	0.062
8	caproic acid	4.5e3	4.5e2	27.5		72.0	0.037
9	succinic acid	119.1	55.1	64.2	1.8	72.0	0.024
10	malic acid	35.2	15.7	66.2	0.9	72.0	0.021
11	caprylic acid	4.2e4	7.8e3	28.8		72.0	0.714
12	adipic acid	596.2	228.0	60.8	2.3	72.0	0.09
13	pelargonic acid	2.0e5	2.2e4	27.9		72.0	0.412
14	citric acid	87.8	48.7	65.1	1.0	72.0	0.067
15	ricinoleic acid	1.9e6	4.8e5	32.9	1.7	72.0	0.421
16	arachidonic acid	5.2e6	1.5e6	29.0	2.6	72.0	0.003

Table S1 (continued): Eberhart fit parameters of alcohols, ketones, aldehydes, sugars, amines, surfactants, and macromolecules shown in Fig. 3. Substances with a star correspond to those denoted by a star in Fig. 3. CI_{95} is the 95 % confidence interval of parameters that were fitted. References for σ_i values that have been measured (i.e., that have no CI_{95} value) can be found in El Haber et al. (2024). RMSE is the root mean square error.

No.	name	S_{1i}	$CI_{95}(S_{1i})$	σ_i (mN m^{-1})	$CI_{95}(\sigma_i)$ (mN m^{-1})	σ_1 (mN m^{-1})	RMSE (mN m^{-1})
17	methanol	7.3	0.3	23.5		72.0	0.016
18	ethanol	20.1	0.8	22.2		72.0	0.458
19	acetone	24.7	2.4	23.5		72.0	0.385
20	propan-1-ol	95.0	7.0	24.0		72.0	0.394
21	propan-2-ol	69.8	7.6	23.5		72.0	0.734
22	ethylene glycol	6.6	0.5	46.6		72.0	0.038
23	propylene glycol	14.8	0.8	35.9		72.0	0.07
24	propane-1,3-diol	12.8	2.2	46.3		72.0	0.216
25	pentan-1-ol	1.3e3	1.4e2	25.2		72.0	0.105
26	1,3-butanediol	27.2	3.1	37.0		72.0	0.291
27	1,4-butanediol	22.9	3.6	43.8		72.0	0.275
28	glycerol	4.4	0.9	63.0		72.0	0.031
29	hexan-1-ol	4.3e3	4.5e2	25.8		72.0	0.028
30	hexan-2-ol	2.6e3	1.1e2	24.5		72.0	0.374
31	2,3-dimethylbutan-2-ol	1.2e3	9.7e1	23.7		72.0	0.753
32	2-methylpentan-2-ol	1.8e3	1.1e2	23.7		72.0	0.317
33	1,5-pentanediol	355.2	175.9	44.2		72.0	0.22
34	heptan-1-ol	2.3e4	3.9e3	26.6		72.0	0.108
35	hexane-1,2-diol	707.7	69.7	23.8		72.0	0.364
36	hexane-1,6-diol	324.1	38.0	42.3	0.7	72.0	0.061
37	hexane-1,5-diol	234.3	31.5	33.9		72.0	0.042
38	hexane-2,5-diol	132.0	20.1	31.6		72.0	0.522
39	octan-1-ol	3.6e4	8.8e3	27.2		72.0	0.144
40	2,3-dihydroxynaphthalene	5.2e4	8.3e3	48.2	1.0	72.0	0.006
41	colamine	6.8	1.2	48.4		72.0	0.258
42	pyrrolidine	25.3	6.9	29.7		72.0	1.223
43	threamine	9.8	2.5	37.4		72.0	0.351
44	3-aminopropan-1-ol	6.5	0.5	44.3		72.0	0.046
45	2-(methylamino)ethan-1-ol	9.6	1.3	35.3		72.0	0.208
46	piperidine	108.1	37.0	29.5		72.0	1.051
47	2-(ethylamino)ethan-1-ol	26.6	8.5	32.2		72.0	1.108
48	cyclohexanamine	885.3	140.5	32.1		72.0	0.741
49	diolamine	9.8	2.3	47.2		72.0	0.035
50	methyl diethanolamine	19.3	2.4	38.2		72.0	0.164
51	DL-norleucine	568.3	561.2	68.1	2.4	72.0	0.016
52	hexamethylenetetramine	117.8	6.8	62.3	0.1	72.0	0.006
53	trolamine	23.1	0.2	46.0		72.0	0.015
54	levoglucosan	45.3	94.0	69.5	2.0	72.0	0.508
55	D-(+)-maltose	9.0	6.7	63.9	4.8	72.0	0.009
★	SDS	1.4e4	2.7e3	29.0	2.6	72.0	0.591
56	DTAB	8.3e3	2.1e3	28.6	3.6	72.0	0.579
57	CTAB	1.5e5	1.9e4	29.2	1.8	72.0	0.259
58	AOT	1.3e5	2.1e4	27.6	1.4	72.0	0.301
59	Triton X114	5.5e6	1.6e6	30.2	1.4	72.0	0.528
60	Brij35	5.5e6	1.4e6	43.7	1.2	72.0	0.165
61	mono-rhamnolipid	7.7e6	2.7e6	27.0	2.9	72.0	0.858
62	di-rhamnolipid	7.0e6	1.8e6	30.4	2.1	72.0	0.434
63	surfactin	1.4e7	7.7e6	27.9	5.6	72.0	0.191
64	syringafactin B/C	4.3e5	1.8e5	19.7	6.2	72.0	0.609
65	viscosin	8.4e6	4.2e6	23.9	5.8	72.0	0.359
66	Suwannee river fulvic acid	1.3e4	3.7e3	39.9	2.7	72.0	0.276
67	NAFA	8.5e4	3.3e4	45.1	5.0	72.0	0.156
68	Humic acid	1.7e4	1.4e4	54.0	3.9	72.0	0.045
69	HULIS	1.9e5	1.6e5	45.5	5.9	72.0	0.229
70	Macromolecules EPS	5.4e7	3.1e7	56.0	2.6	72.0	0.209

S7 Surface tension isotherms of atmospheric samples

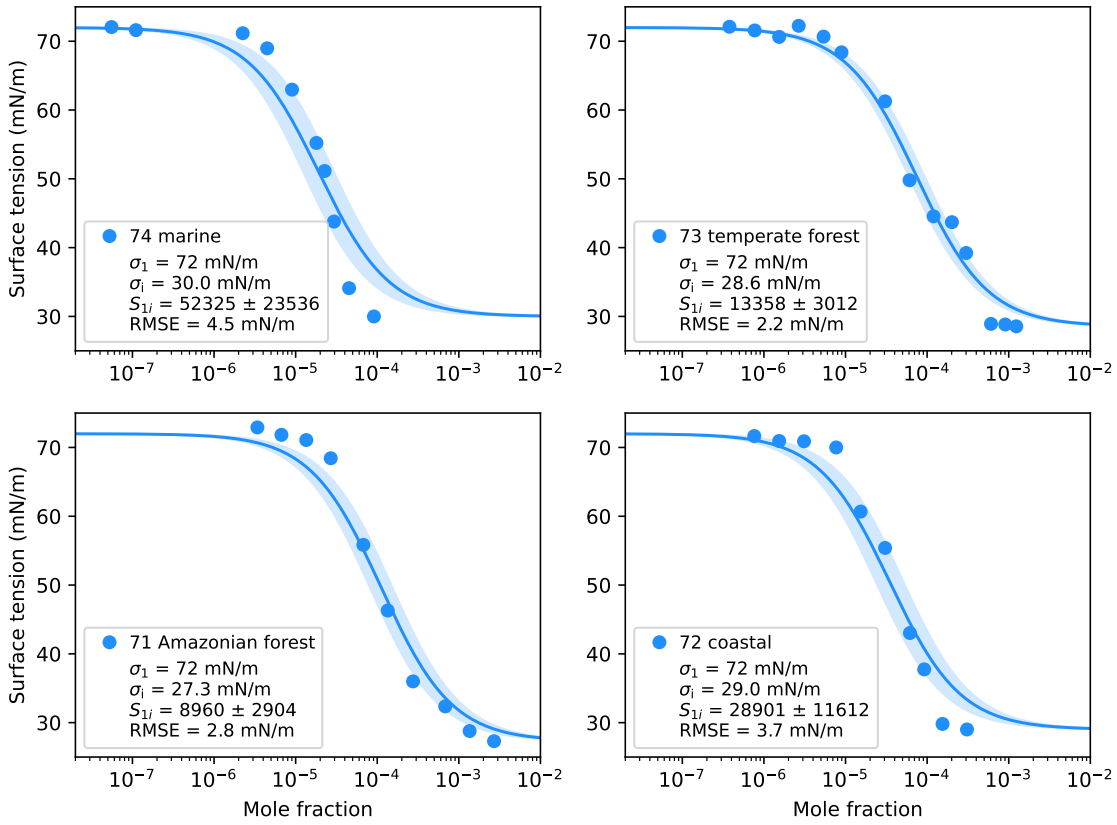

Figure S8: Eberhart model (Eq. 3) fits (solid lines) to surface tension data (markers) of atmospheric sample extracts from Ekström et al. (2010) taken at four different locations. Numbers 71–74 refer to the numbering in Fig. 3. Colored shading shows the 95 % confidence interval. In the legend, the model parameters are given. σ_1 was set to 72 mN m^{-1} for all samples and σ_i was taken to be the minimum of the experimental data. S_{1i} was fitted and its 95 % confidence interval is given as the uncertainty. RMSE is the root mean square error.

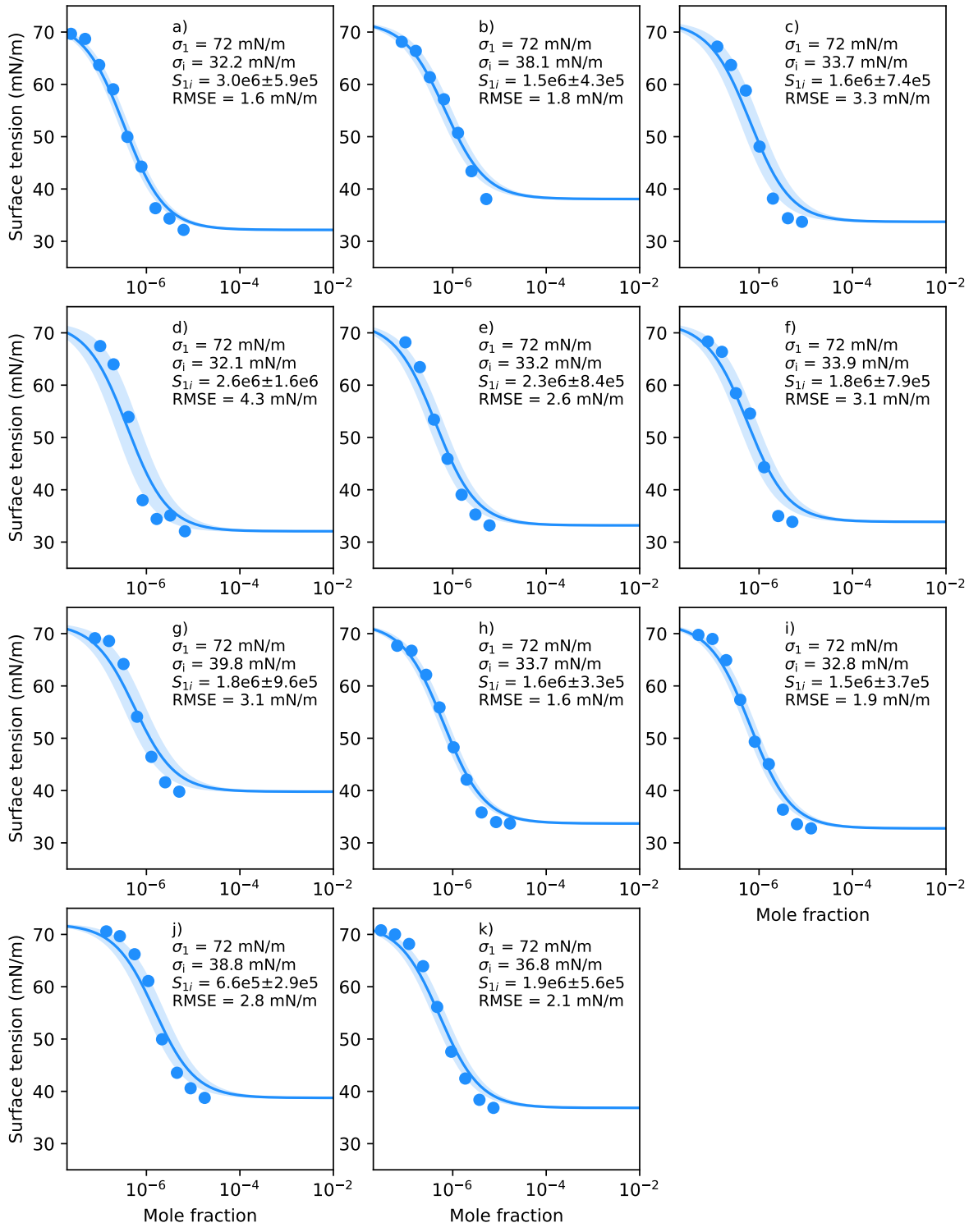

Figure S9: Eberhart model (Eq. 3) fits (solid lines) to surface tension data (markers) of 11 atmospheric sample extracts (a–k) from Gérard et al. (2016) taken at the Baltic Coast at Askö in Sweden. Colored shading shows the 95 % confidence interval. In each panel, the model parameters are shown. σ_1 was set to 72 mN m^{-1} for all samples and σ_i was taken to be the minimum of the experimental data. S_{1i} was fitted and its 95 % confidence interval is given as the uncertainty. RMSE is the root mean square error.

S8 Surface tension isotherms of the model compounds

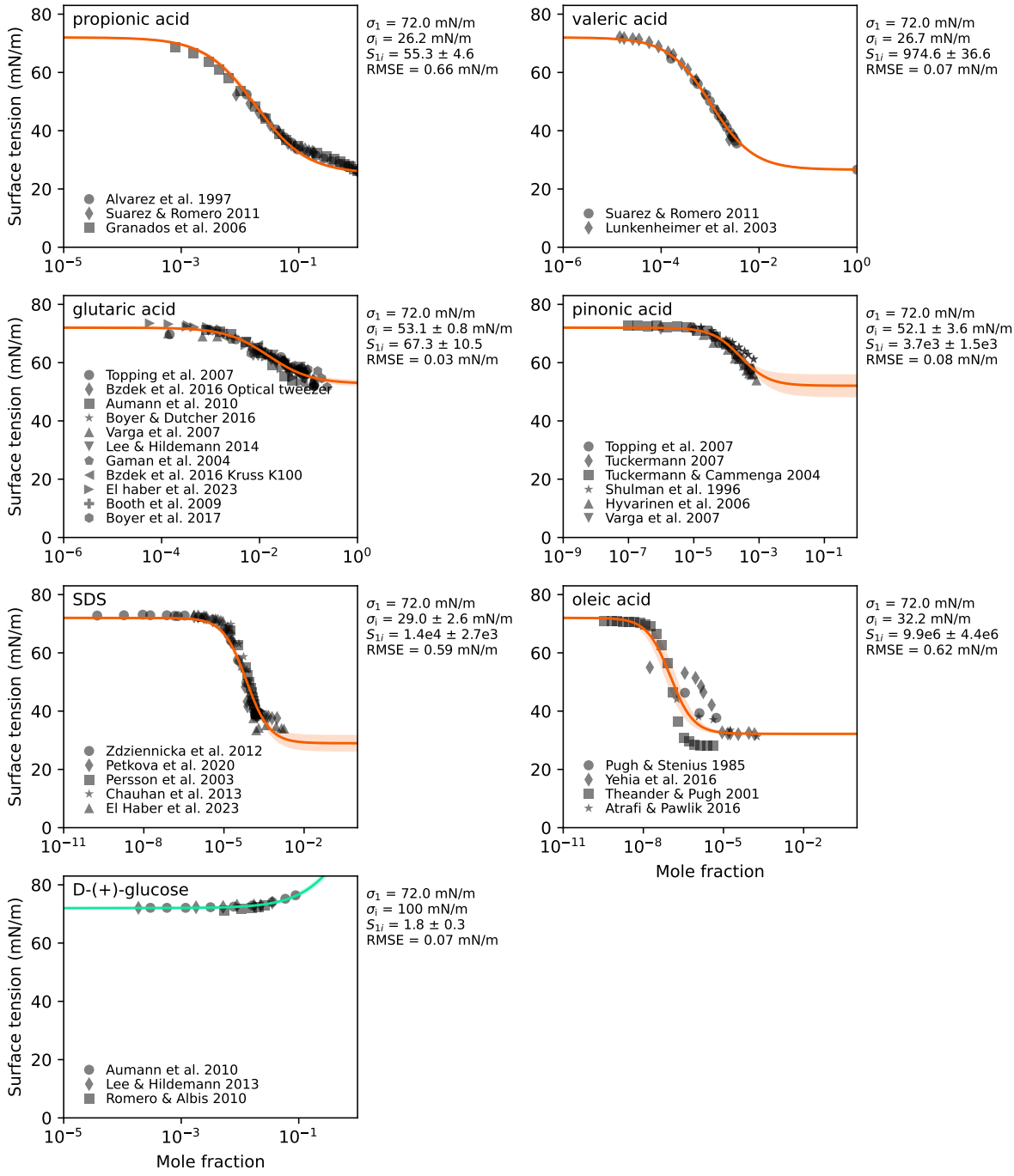

Figure S10: Binary surface tension data (black markers) and Eberhart model fits (colored solid lines) for the model compounds in this study. Fit parameters are annotated in the respective panel together with the root mean square error (RMSE). The colored shading represents the 95 % confidence interval of the fit. Different markers represent different datasets. For further information on the underlying data refer to El Haber et al. (2024). For NaCl, refer to Kleinheins et al. (2023).

S9 Influence of salting-out

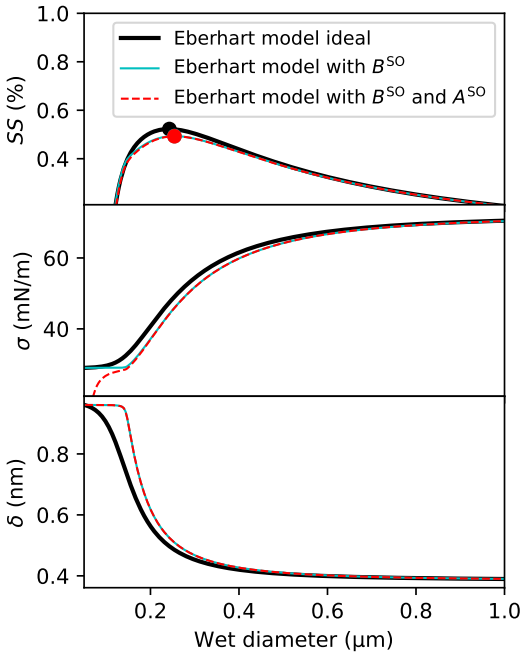

Figure S11: Influence of surface tension non-ideality (salting-out) on the Köhler curve (first row) and critical supersaturation (circle), droplet surface tension σ (second row), and the monolayer thickness δ (third row), using an artificially high salting-out factor of $B_{24}^{SO} = 10^5$. Three cases are distinguished: assuming ideality (solid black lines, $A_{24}^{SO} = 0$,$B_{24}^{SO} = 0$), considering bulk related salting-out (solid cyan lines $A_{24}^{SO} = 0$, $B_{24}^{SO} = 10^5$), and considering bulk and surface related salting-out (dashed red line, $A_{24}^{SO} = 22.63$, $B_{24}^{SO} = 10^5$). In all cases, $D_{dry} = 50\,nm$, $w_{org} = 0.93$ ("med"), and $w_{glu}/w_{org} = 0$.

S10 Influence of SDS density

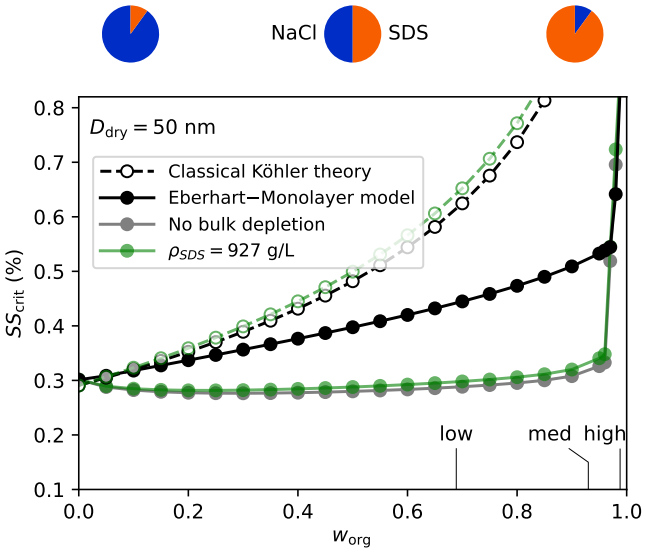

Figure S12: Influence of the SDS density on the results in Fig. 5. Black and gray data is calculated using $\rho_{SDS} = 1030\,g\,L^{-1}$ and green data is calculated using a 10 % lower density, i.e., $\rho_{SDS} = 927\,g\,L^{-1}$.

S11 Köhler curves of additional systems

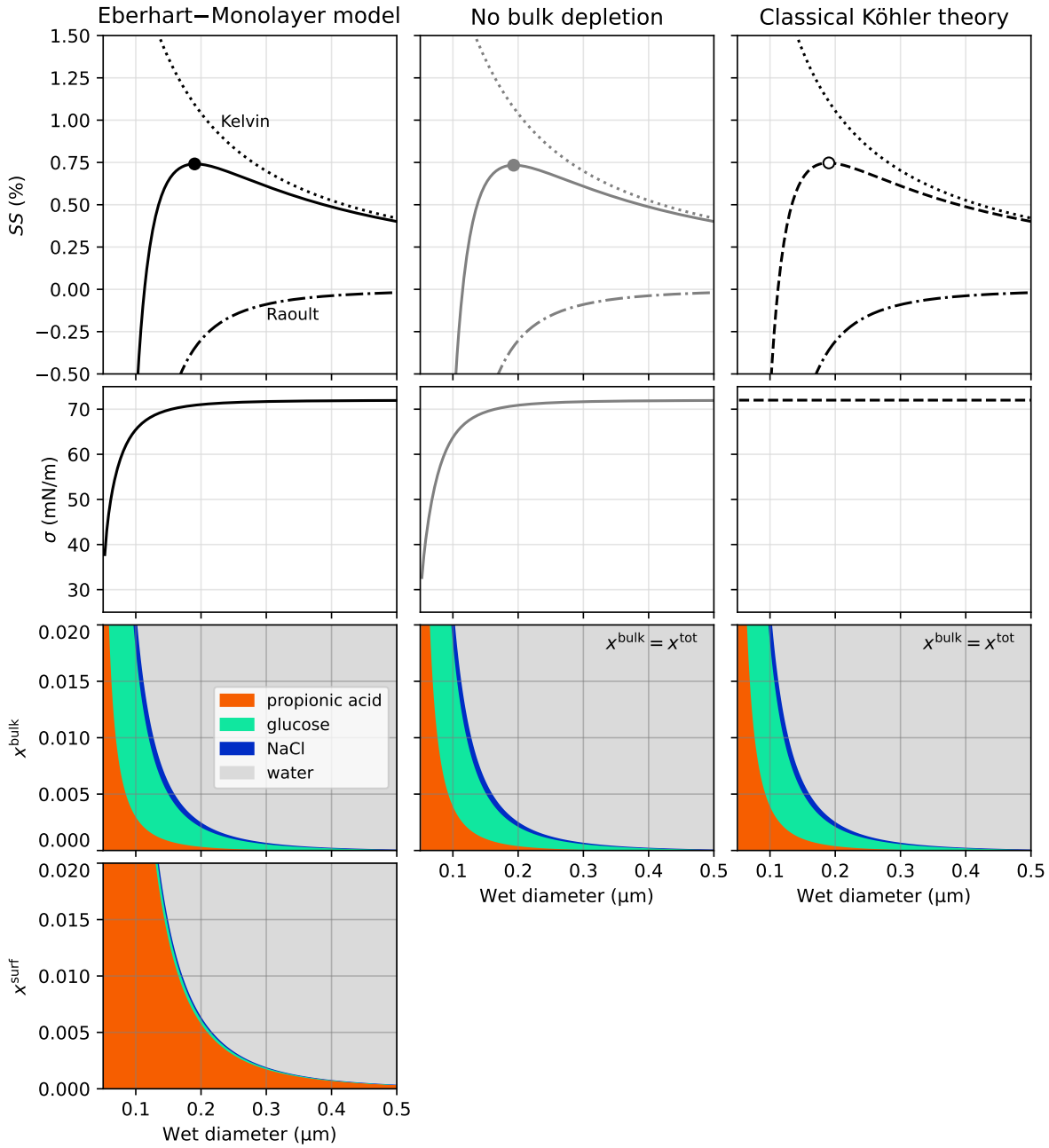

Figure S13: Same as Fig. 4 but using propionic acid instead of SDS and a high fraction of glucose ($w_{glu}/w_{org} = 0.9$). In the third and fourth row, the y-axis range was limited to 0–0.02 for a better visibility of the solute share.

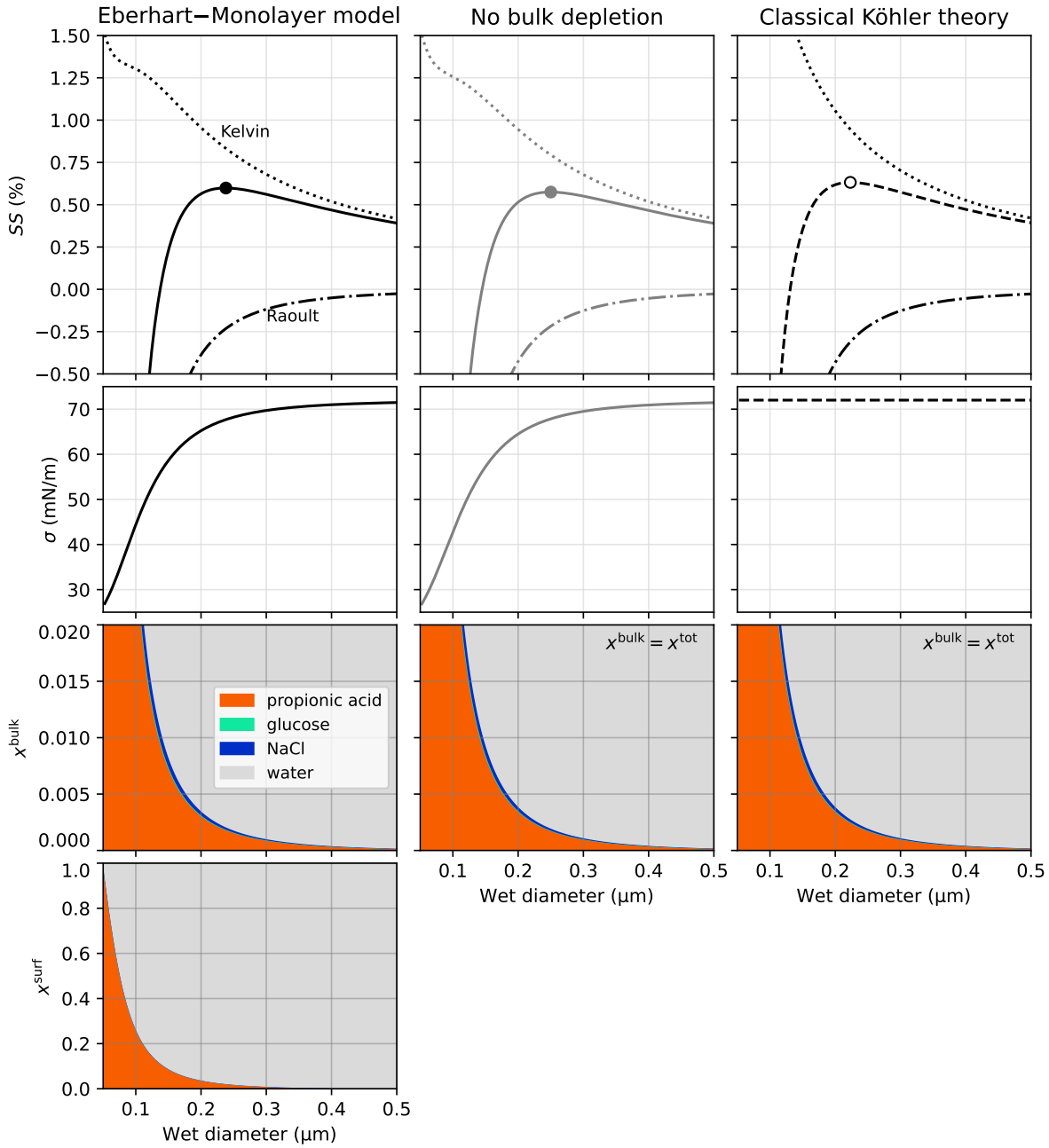

Figure S14: Same as Fig. 4 but using propionic acid instead of SDS.

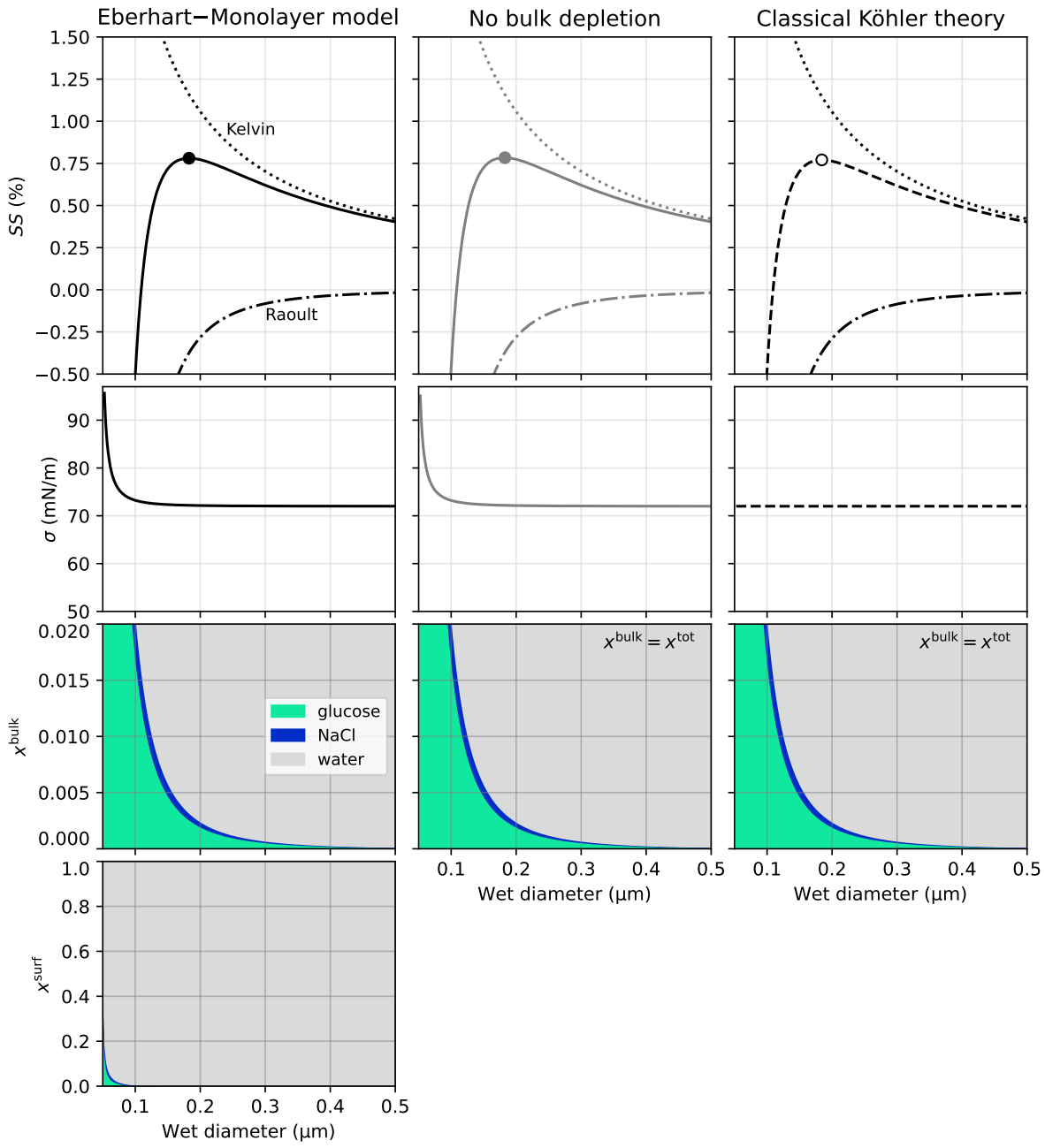

Figure S15: Köhler curves calculated with the Eberhart–Monolayer model, assuming no bulk depletion, and with Classical Köhler theory for a ternary glucose–NaCl–water particle (i.e., $w_{glu}/w_{org} = 1$) with $D_{dry} = 50\,nm$ and $w_{org} = 0.93$ ("med"). First row: Köhler curve (solid or dashed line) with Raoult (dash-dotted lines) and Kelvin effect (dotted lines) and critical supersaturation (circle). Second row: droplet surface tension. Third row: bulk composition (first column) and total composition (second and third column). The y-axis range was limited to 0–0.02 for a better visibility of the solute share. Fourth row: surface composition in the Eberhart–Monolayer model. For consistency with the previous plots, the y-axis range is kept here at 0–1. Since no partitioning is calculated in the second and third column, the surface composition is not determined and hence not shown here.

S12 Variation of the surfactant

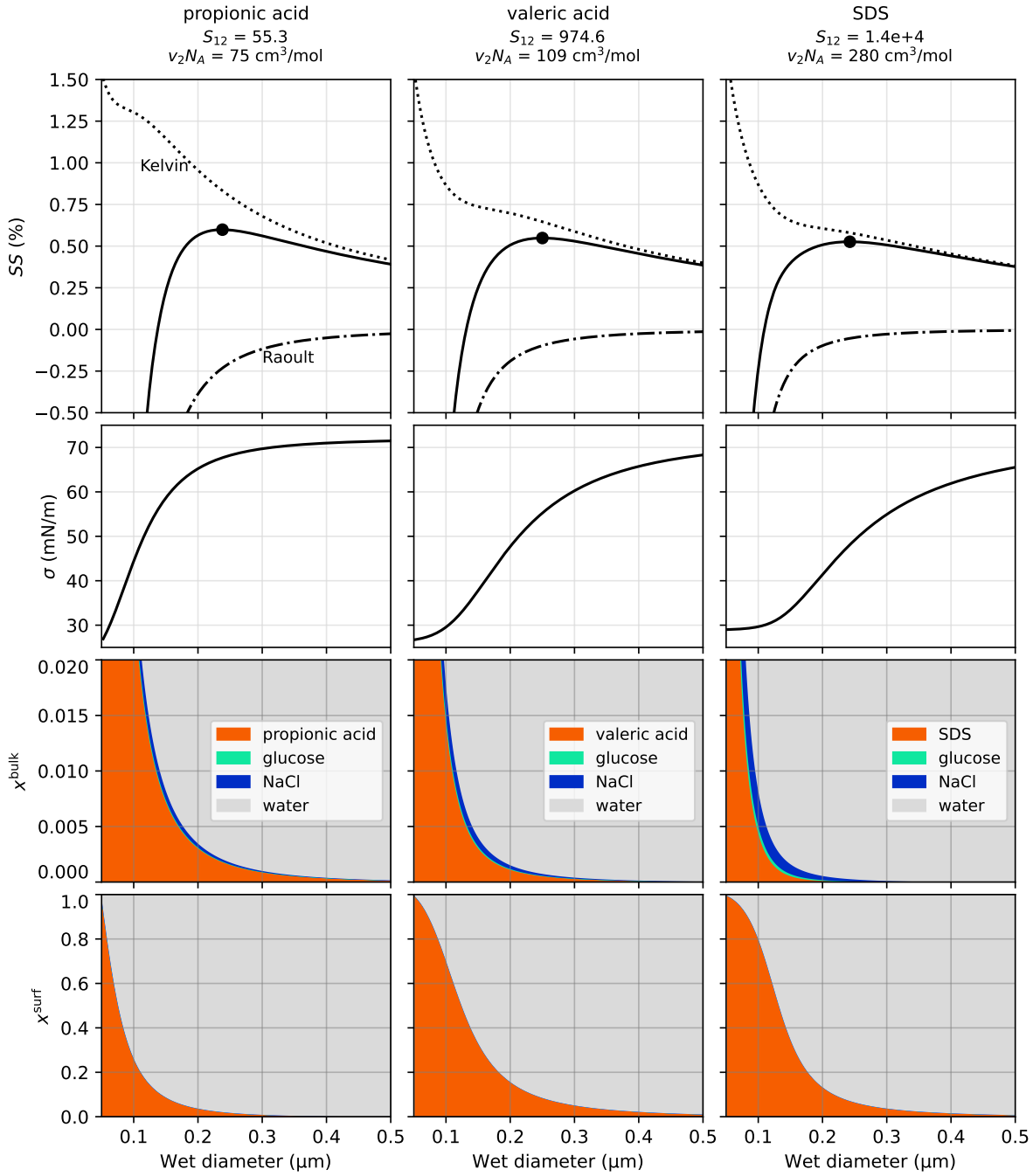

Figure S16: Köhler curves to illustrate the effect of molar volume v_2N_A on the Raoult effect and separation factor S_{12} on the Kelvin effect calculated with the Eberhart–Monolayer model for three different surfactants in a quaternary surfactant–glucose–NaCl–water particle ($D_{\mathrm{dry}} = 50\,\mathrm{nm}$, $w_{\mathrm{org}} = 0.93$ ("med"), and $w_{\mathrm{glu}}/w_{\mathrm{org}} = 0.05$). First row: Köhler curve (solid or dashed line) with Raoult (dash-dotted lines) and Kelvin effect (dotted lines) and critical supersaturation (circle), second row: droplet surface tension, third row: bulk composition, and fourth row: surface composition. The y-axis range in the third row was limited to 0–0.02 for a better visibility of the solute share.

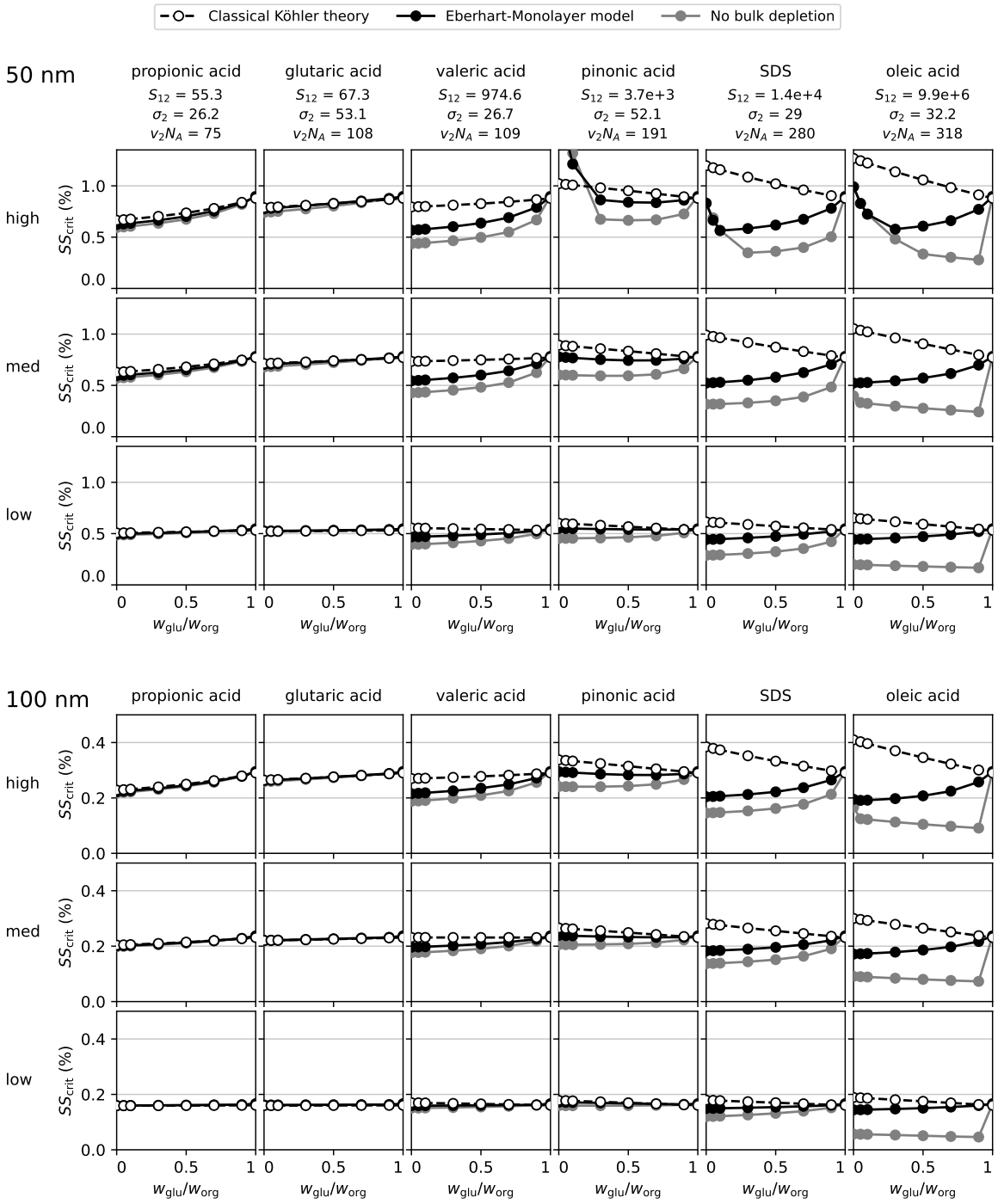

Figure S17: Combined influence of surfactant properties and the organic fraction on critical supersaturation for two different particle sizes. Upper panel: $D_{dry} = 50\,nm$. Lower panel: $D_{dry} = 100\,nm$. In the column title, the name of the surfactant, its binary separation factor in water S_{12}, its pure component surface tension in $mN\,m^{-1}$, and its molar volume in $cm^3\,mol^{-1}$ is given. The organic fraction w_{org} for each row can be found in Table 1. In some of the calculations with glutaric acid and propionic acid all curves overlap.

S13 Influence of organic fraction on the critical activation diameter

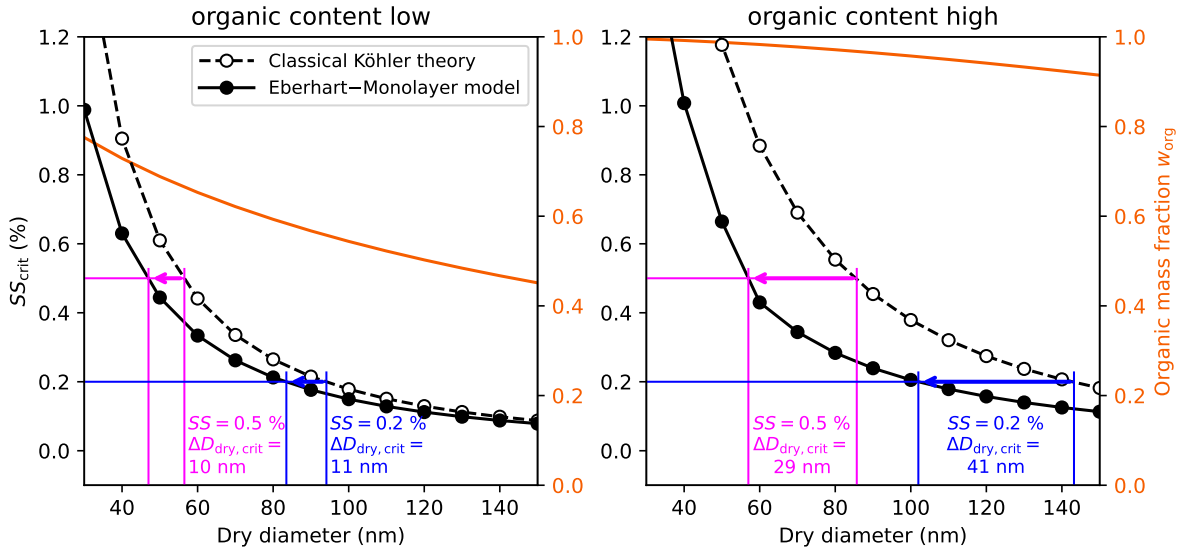

Figure S18: Same as Fig. 8 but with low organic content (left panel) and high organic content (right panel). The organic fraction is shown with an orange solid line on the right y-axis.

References

Alvarez, E., Vázquez, G., Sánchez-Vilas, M., Sanjurjo, B., and Navaza, J. M.: Surface Tension of Organic Acids + Water Binary Mixtures from 20 °C to 50 °C, J. Chem. Eng. Data, 42, 957–960, https://doi.org/10.1021/je970025m, 1997.

Atrafi, A. and Pawlik, M.: Surface tension and gas dispersion properties of fatty acid solutions, Minerals Engineering, 85, 138–147, https://doi.org/10.1016/j.mineng.2015.11.006, 2016.

Aumann, E., Hildemann, L., and Tabazadeh, A.: Measuring and modeling the composition and temperature-dependence of surface tension for organic solutions, Atmospheric Environment, 44, 329–337, https://doi.org/10.1016/j.atmosenv.2009.10.033, 2010.

Bain, A., Ghosh, K., Prisle, N. L., and Bzdek, B. R.: Surface-Area-to-Volume Ratio Determines Surface Tensions in Microscopic, Surfactant-Containing Droplets, ACS Central Science, 9, 2076–2083, https://doi.org/10.1021/acscentsci.3c00998, 2023.

Booth, A. M., Topping, D. O., McFiggans, G., and Percival, C. J.: Surface tension of mixed inorganic and dicarboxylic acid aqueous solutions at 298.15 K and their importance for cloud activation predictions, Phys. Chem. Chem. Phys., 11, 8021–8028, https://doi.org/10.1039/B906849J, 2009.

Boyer, H. C. and Dutcher, C. S.: Statistical Thermodynamic Model for Surface Tension of Aqueous Organic Acids with Consideration of Partial Dissociation, The Journal of Physical Chemistry A, 120, 4368–4375, https://doi.org/10.1021/acs.jpca.6b01469, pMID: 27219322, 2016.

Boyer, H. C., Bzdek, B. R., Reid, J. P., and Dutcher, C. S.: Statistical Thermodynamic Model for Surface Tension of Organic and Inorganic Aqueous Mixtures, The Journal of Physical Chemistry A, 121, 198–205, https://doi.org/10.1021/acs.jpca.6b10057, pMID: 27933984, 2017.

Bzdek, B. R., Power, R. M., Simpson, S. H., Reid, J. P., and Royall, C. P.: Precise, contactless measurements of the surface tension of picolitre aerosol droplets, Chem. Sci., 7, 274–285, https://doi.org/10.1039/C5SC03184B, 2016.

Chauhan, S., Sharma, V., and Sharma, K.: Maltodextrin–SDS interactions: Volumetric, viscometric and surface tension study, Fluid Phase Equilibria, 354, 236–244, https://doi.org/10.1016/j.fluid.2013.06.051, 2013.

Ekström, S., Nozière, B., Hultberg, M., Alsberg, T., Magnér, J., Nilsson, E. D., and Artaxo, P.: A possible role of ground-based microorganisms on cloud formation in the atmosphere, Biogeosciences, 7, 387–394, https://doi.org/10.5194/bg-7-387-2010, 2010.

El Haber, M., Ferronato, C., Giroir-Fendler, A., Fine, L., and Nozière, B.: Salting out, non-ideality and synergism enhance surfactant efficiency in atmospheric aerosols, Scientific Reports, 13, 20 672, https://doi.org/10.1038/s41598-023-48040-5, 2023.

El Haber, M., Gérard, V., Kleinheins, J., Ferronato, C., and Nozière, B.: Measuring the Surface Tension of Atmospheric Particles and Relevant Mixtures to Better Understand Key Atmospheric Processes, Chem. Rev., 124, 10 924–10 963, https://doi.org/10.1021/acs.chemrev.4c00173, 2024.

Gaman, A. I., Kulmala, M., Vehkamäki, H., Napari, I., Mircea, M., Facchini, M. C., and Laaksonen, A.: Binary homogeneous nucleation in water–succinic acid and water–glutaric acid systems, The Journal of Chemical Physics, 120, 282–291, https://doi.org/10.1063/1.1630564, 2004.

Granados, K., Gracia-Fadrique, J., Amigo, A., and Bravo, R.: Refractive Index, Surface Tension, and Density of Aqueous Mixtures of Carboxylic Acids at 298.15 K, Journal of Chemical & Engineering Data, 51, 1356–1360, https://doi.org/10.1021/je060084c, 2006.

Gérard, V., Nozière, B., Baduel, C., Fine, L., Frossard, A. A., and Cohen, R. C.: Anionic, Cationic, and Nonionic Surfactants in Atmospheric Aerosols from the Baltic Coast at Askö, Sweden: Implications for Cloud Droplet Activation, Environmental Science & Technology, 50, 2974–2982, https://doi.org/10.1021/acs.est.5b05809, 2016.

Hyvärinen, A.-P., Lihavainen, H., Gaman, A., Vairila, L., Ojala, H., Kulmala, M., and Viisanen, Y.: Surface Tensions and Densities of Oxalic, Malonic, Succinic, Maleic, Malic, and cis-Pinonic Acids, Journal of Chemical & Engineering Data, 51, 255–260, https://doi.org/10.1021/je050366x, 2006.

Kleinheins, J., Shardt, N., El Haber, M., Ferronato, C., Nozière, B., Peter, T., and Marcolli, C.: Surface tension models for binary aqueous solutions: a review and intercomparison, Phys. Chem. Chem. Phys., 25, 11 055–11 074, https://doi.org/10.1039/D3CP00322A, 2023.

Lee, J. Y. and Hildemann, L. M.: Surface tension of solutions containing dicarboxylic acids with ammonium sulfate, d-glucose, or humic acid, Journal of Aerosol Science, 64, 94–102, https://doi.org/10.1016/j.jaerosci.2013.06.004, 2013.

Lee, J. Y. and Hildemann, L. M.: Surface tensions of solutions containing dicarboxylic acid mixtures, Atmospheric Environment, 89, 260–267, https://doi.org/10.1016/j.atmosenv.2014.02.049, 2014.

Lunkenheimer, K., Barzyk, W., Hirte, R., and Rudert, R.: Adsorption Properties of Soluble, Surface-Chemically Pure n-Alkanoic Acids at the Air/Water Interface and the Relationship to Insoluble Monolayer and Crystal Structure Properties, Langmuir, 19, 6140–6150, https://doi.org/10.1021/la034379p, 2003.

Matijević, E. and Pethica, B. A.: The properties of ionized monolayers. Part 1.—Sodium dodecyl sulphate at the air/water interface, Trans. Faraday Soc., 54, 1382–1389, https://doi.org/10.1039/TF9585401382, 1958.

Persson, C., Jonsson, A., Bergström, M., and Eriksson, J. C.: Testing the Gouy–Chapman theory by means of surface tension measurements for SDS–NaCl–H2O mixtures, Journal of Colloid and Interface Science, 267, 151–154, https://doi.org/10.1016/S0021-9797(03)00761-6, 2003.

Petkova, B., Tcholakova, S., Chenkova, M., Golemanov, K., Denkov, N., Thorley, D., and Stoyanov, S.: Foamability of aqueous solutions: Role of surfactant type and concentration, Advances in Colloid and Interface Science, 276, 102 084, https://doi.org/10.1016/j.cis.2019.102084, 2020.

Prisle, N. L., Raatikainen, T., Laaksonen, A., and Bilde, M.: Surfactants in cloud droplet activation: mixed organic-inorganic particles, Atmospheric Chemistry and Physics, 10, 5663–5683, https://doi.org/10.5194/acp-10-5663-2010, 2010.

Pugh, R. and Stenius, P.: Solution chemistry studies and flotation behaviour of apatite, calcite and fluorite minerals with sodium oleate collector, International Journal of Mineral Processing, 15, 193–218, https://doi.org/10.1016/0301-7516(85)90035-3, 1985.

Romero, C. M. and Albis, A.: Influence of Polyols and Glucose on the Surface Tension of Bovine alpha-Lactalbumin in Aqueous Solution, Journal of Solution Chemistry, 39, 1865–1876, https://doi.org/10.1007/s10953-010-9554-5, 2010.

Shulman, M. L., Jacobson, M. C., Carlson, R. J., Synovec, R. E., and Young, T. E.: Dissolution behavior and surface tension effects of organic compounds in nucleating cloud droplets, Geophysical Research Letters, 23, 277–280, https://doi.org/10.1029/95GL03810, 1996.

Sorjamaa, R., Svenningsson, B., Raatikainen, T., Henning, S., Bilde, M., and Laaksonen, A.: The role of surfactants in Köhler theory reconsidered, Atmospheric Chemistry and Physics, 4, 2107–2117, https://doi.org/10.5194/acp-4-2107-2004, 2004.

Suárez, F. and Romero, C. M.: Apparent Molar Volume and Surface Tension of Dilute Aqueous Solutions of Carboxylic Acids, Journal of Chemical & Engineering Data, 56, 1778–1786, https://doi.org/10.1021/je1002829, 2011.

Theander, K. and Pugh, R. J.: The Influence of pH and Temperature on the Equilibrium and Dynamic Surface Tension of Aqueous Solutions of Sodium Oleate, Journal of Colloid and Interface Science, 239, 209–216, https://doi.org/10.1006/jcis.2000.7543, 2001.

Topping, D. O., McFiggans, G. B., Kiss, G., Varga, Z., Facchini, M. C., Decesari, S., and Mircea, M.: Surface tensions of multi-component mixed inorganic/organic aqueous systems of atmospheric significance: measurements, model predictions and importance for cloud activation predictions, Atmospheric Chemistry and Physics, 7, 2371–2398, https://doi.org/10.5194/acp-7-2371-2007, 2007.

Tuckermann, R.: Surface tension of aqueous solutions of water-soluble organic and inorganic compounds, Atmospheric Environment, 41, 6265–6275, https://doi.org/10.1016/j.atmosenv.2007.03.051, 2007.

Tuckermann, R. and Cammenga, H. K.: The surface tension of aqueous solutions of some atmospheric water-soluble organic compounds, Atmospheric Environment, 38, 6135–6138, https://doi.org/10.1016/j.atmosenv.2004.08.005, 2004.

Varga, Z., Kiss, G., and Hansson, H.-C.: Modelling the cloud condensation nucleus activity of organic acids on the basis of surface tension and osmolality measurements, Atmospheric Chemistry and Physics, 7, 4601–4611, https://doi.org/10.5194/acp-7-4601-2007, 2007.

Yehia, A., El-Halim, S. A., Sharada, H., Khalek, M. A., and Ammar, M.: Interactions of Cellulase and Oleic Acid Solution Mixtures, Tenside Surfactants Detergents, 53, 176–181, https://doi.org/10.3139/113.110423, 2016.

Zdziennicka, A., Szymczyk, K., Krawczyk, J., and Jańczuk, B.: Activity and thermodynamic parameters of some surfactants adsorption at the water–air interface, Fluid Phase Equilibria, 318, 25–33, https://doi.org/10.1016/j.fluid.2012.01.014, 2012.